Editors' Suggestion

Extreme Fermi Surface Smearing in a Maximally Disordered Concentrated Solid Solution

Hannah C. Robarts,[1] Thomas E. Millichamp,[1] Daniel A. Lagos,[1] Jude Laverock,[1] David Billington,[2,3] Jonathan A. Duffy,[4] Daniel O'Neill,[4] Sean R. Giblin,[3] Jonathan W. Taylor,[5] Grazyna Kontrym-Sznajd,[6] Małgorzata Samsel-Czekała,[6] Hongbin Bei,[7] Sai Mu,[7] German D. Samolyuk,[7] G. Malcolm Stocks,[7] and Stephen B. Dugdale[1,*]

[1]*H.H. Wills Physics Laboratory, University of Bristol, Tyndall Avenue, Bristol BS8 1TL, United Kingdom*
[2]*Japan Synchrotron Radiation Research Institute, SPring-8, Sayo 679-5198, Japan*
[3]*School of Physics and Astronomy, Cardiff University, Queen's Building, The Parade, Cardiff CF24 3AA, United Kingdom*
[4]*Department of Physics, University of Warwick, Coventry CV4 7AL, United Kingdom*
[5]*DMSC—European Spallation Source, Universitetsparken 1, Copenhagen 2100, Denmark*
[6]*Institute of Low Temperature and Structure Research, Polish Academy of Sciences, PO Box 1410, 50-950 Wrocław 2, Poland*
[7]*Materials Science and Technology Division, Oak Ridge National Laboratory, Oak Ridge, Tennessee 37831, USA*

(Received 9 September 2019; revised manuscript received 20 December 2019; published 30 January 2020)

We show that the Fermi surface can survive the presence of extreme compositional disorder in the equiatomic alloy $Ni_{0.25}Fe_{0.25}Co_{0.25}Cr_{0.25}$. Our high-resolution Compton scattering experiments reveal a Fermi surface which is smeared across a significant fraction of the Brillouin zone (up to 40% of $2\pi/a$). The extent of this smearing and its variation on and between different sheets of the Fermi surface have been determined, and estimates of the electron mean free path and residual resistivity have been made by connecting this smearing with the coherence length of the quasiparticle states.

DOI: 10.1103/PhysRevLett.124.046402

The emergence of the Fermi surface (FS) from the theory of the electronic structure of metals, together with the pioneering experimental determinations of its shape, stand proudly among the greatest achievements of twentieth century physics [1]. The FS, defined by the discontinuity in the momentum distribution, exists even for interacting electrons [2,3], and here we demonstrate its remarkable ability to survive maximal compositional disorder in which the electron mean free path (which we can also extract from our measurements) is comparable to the lattice spacing. In disordered systems, the Mott-Ioffe-Regel (MIR) limit describes the semiclassical upper bound for coherent transport in a metal, occurring when the electron mean free path becomes comparable with the interatomic spacing [4]. The modern description of the electronic structure of crystalline solids—the band theory of electrons—depends on the notion of perfect crystals exhibiting long-range order. The Bloch wave functions which emerge are a direct consequence of the discrete translational invariance of the potential experienced by the electrons traveling through the ionic lattice. This premise is strongly challenged in substitutionally disordered random alloys (concentrated solid solutions) where there is no such periodicity. Abandoning the familiar concepts associated with a well-defined reciprocal lattice, such as the Brillouin zone (BZ) and indeed the FS, seems inevitable. However, there is considerable theoretical and experimental evidence (e.g., Refs. [5,6]) that by considering an *ordered* system comprising suitably chosen effective scatterers to restore periodicity, the BZ and FS can be resurrected. The resulting electron states, however, have finite lifetimes due to the presence of disorder, and the "bands" are smeared in both energy, E (resulting in a finite electron lifetime) and crystal momentum, $\mathbf{k}$ (finite mean free path). This also means that the discontinuity in the momentum distribution associated with the FS is also smeared out in both E and $\mathbf{k}$, with correspondingly reduced Fermi energy electron lifetimes and short mean free paths. A sharp FS in an ultrapure metal at cryogenic temperatures is associated with electron mean free paths of more than a centimeter [7]. While bulk resistivities of metals are rather well known, comparatively little *direct* information exists about electron mean free paths [8].

A new class of metallic alloys, referred to as "high entropy alloys" (with the terms "multiprincipal element alloys" and "complex concentrated alloys" being used in a broader sense [9]), has recently been introduced. These alloys consist of approximately equiatomic concentrations of multiple metallic elements and are thus fundamentally different from traditional alloys which have one principal component. The Cantor-Wu alloys are particularly interesting examples [10,11]. While these alloys form on a face-centered-cubic lattice and the atoms have relatively small deviations from their ideal lattice positions (small displacement fluctuations [12]), the chemical (compositional) disorder is considerable leading to a smeared electronic structure [13,14]. The lattice vibrations are also expected to be scattered by the disorder, leading to broadening of the phonon linewidths due to a shortened lifetime [15]. In spite of such disorder, superconductivity was recently observed

in a refractory (bcc) high entropy alloy [16], implying the existence of a FS.

In this Letter we present an experimental measurement of the FS of a maximally disordered (in the sense that the ideal entropy of mixing is maximal at equiatomic composition) medium entropy alloy, equiatomic $Ni_{0.25}Fe_{0.25}Co_{0.25}Cr_{0.25}$ (henceforth referred to as NiFeCoCr), using high-resolution Compton scattering. Compton scattering is a bulk-sensitive probe of the occupied momentum states in a solid and is thus a particularly powerful technique for measuring the FSs of disordered alloys, it not being limited by short electron mean free paths [17]. We show that a meaningful FS can be identified, in spite of it being smeared across a substantial fraction of the BZ, and that studying the smeared-out FS discontinuity can be used to deduce the electron mean free path. Furthermore, we show that state-of-the-art theory for disordered systems, which generalizes the notion of the FS to systems dominated by disorder, is able to predict correctly the FS topology.

Korringa-Kohn-Rostoker (KKR) calculations which describe both the chemical disorder and the magnetic disorder above the Curie temperature ($T_C \sim 120$ K, the disordered local moment (DLM) state [18,19]) with the mean-field coherent potential approximation (CPA) [20] complement our experiments. The electronic structure can most easily be described through the $\mathbf{k}$-resolved density of states known as the Bloch spectral function (BSF), $A_B(E, \mathbf{k})$ [21]. For a perfectly ordered system, the behavior of $A_B(E, \mathbf{k})$ on passing through a band (in either $\mathbf{k}$ or E) would be a δ function (implying infinite quasiparticle lifetime), but in the presence of weak disorder the line shape is broadened into an approximately Lorentzian form. The KKR-CPA BSF is valid for arbitrarily strong disorder and deals with both the real part of the self-energy (leading to shifts in the band energies) and the imaginary part (which broadens the energy bands). The electronic band structure can be visualized through the BSF, which for NiFeCoCr (Fig. 1) is particularly smeared for states close to the Fermi energy where the energy separation between the flat d bands of the component elements is large on the scale of the corresponding d-band width.

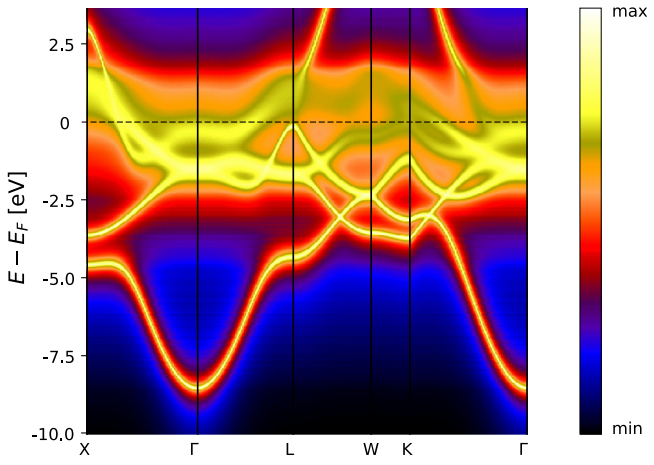

FIG. 1. Logarithm of the Bloch spectral function of NiFeCoCr calculated within the KKR-CPA-DLM framework.

Compton profiles were measured on a single crystal of NiFeCoCr at room temperature along 15 special crystallographic directions [22] using the spectrometer on beam line BL08W at SPring-8 [23]. The full 3D electron momentum density, $\rho(\mathbf{p})$ was reconstructed from the 1D Compton profiles $[J(p_z)]$ by lattice harmonic expansion in the method proposed by Kontrym-Sznajd and Samsel-Czekała [24]. The resulting distribution in $\mathbf{p}$ space was then translated back into the first Brillouin zone (1BZ) by summing contributions separated by a reciprocal lattice vector as prescribed by the Lock-Crisp-West (LCW) theorem [25], thus giving an occupation number $n(\mathbf{k})$ in the 1BZ. The contributions of electrons in fully occupied bands sum to give a constant contribution across the BZ (with an intensity proportional to the number of occupied bands), whereas the signatures of the FS due to electrons in

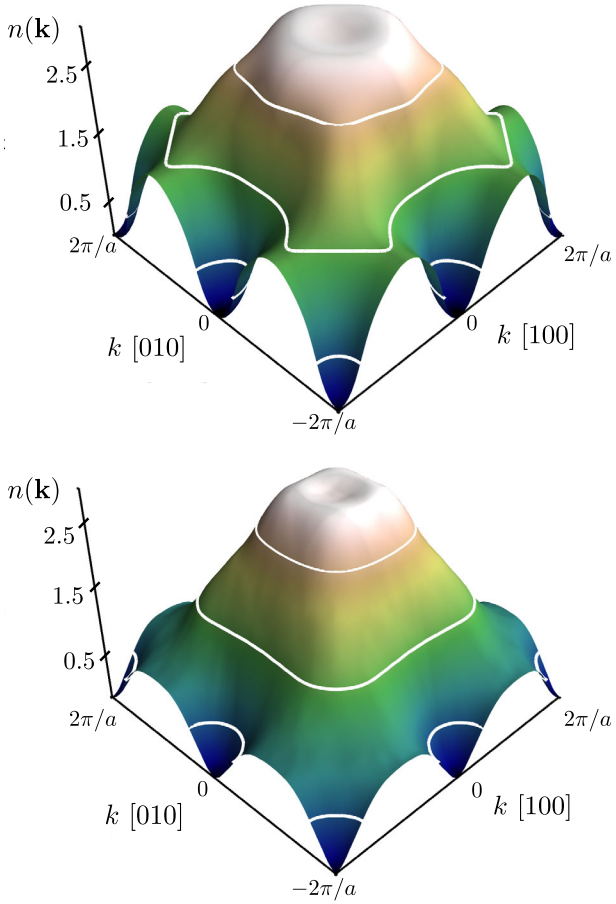

FIG. 2. Occupation $n(\mathbf{k})$ in the (001) plane through Γ, showing the KKR-CPA-DLM theory (top) and experiment (bottom). $2\pi/a \approx 0.93$ a.u., and the white lines indicate the isodensities associated with the three FS sheets.

partially occupied bands reinforce constructively, producing features in $n(\mathbf{k})$ which are steplike discontinuities for a perfectly ordered system, but which are smeared out in a disordered alloy.

From the KKR-CPA-DLM calculations, $n(\mathbf{k})$ can be obtained from an energy integral of the BSF:

$$n(\mathbf{k}) = \int_{-\infty}^{E_F} A_B(E, \mathbf{k}) dE. \quad (1)$$

In Fig. 2, we show $n(\mathbf{k})$ on the (001) plane (through Γ), from both the calculation (top) and experiment (bottom). The topology of the FS can immediately be deduced, with occupied states around the Γ point at the center and hole pockets at the X points (located in the middle of the edges and at the corners). The KKR-CPA-DLM theory predicts three FS sheets, and given that there are regions of the BZ where none of these three bands are occupied and regions where all three are occupied, the dynamic range (minimum to maximum) of $n(\mathbf{k})$ can be normalized to a value of three. For an arbitrary $\mathbf{k}$ point in the BZ, if $n(\mathbf{k}) = 0$, then none of the three bands are occupied, while $n(\mathbf{k}) = 3$ would imply that all three bands are occupied. In this scheme, a set of isodensities at 0.5, 1.5, and 2.5 could be used to visualize the three FS sheets, and these are shown as white lines in Fig. 2. The smearing (there are no sharp steps) is intrinsic to the disorder, the impact of the finite experimental resolution (0.10 a.u.) being very small (see Ref. [26]). However, for ease of comparison, all the theoretical distributions have been convoluted with a function representing the experimental resolution. The qualitative level of agreement is remarkable, with even a small dip around the Γ point (due to a grazing band [26]) appearing in both.

The BSF from the KKR-CPA-DLM calculation is shown in the top half of Fig. 3, with the hole pockets at the X points clearly visible, and the larger Γ-centered electron sheet being rather smeared out, particularly along the ⟨110⟩ directions. To identify both the location and sharpness of

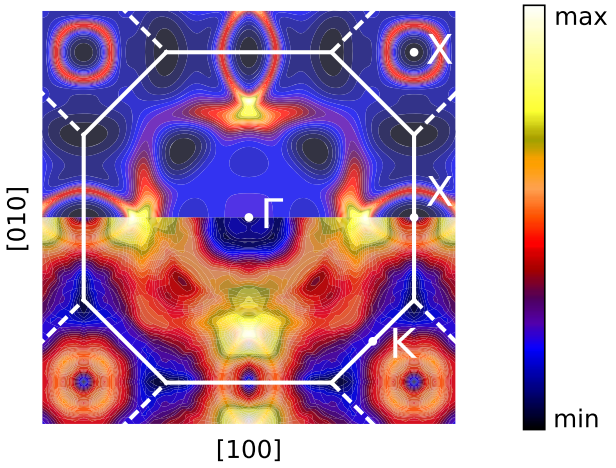

FIG. 3. Bloch spectral function $A_B(E = E_F, \mathbf{k})$ in the (001) plane through Γ from the KKR-CPA-DLM theory (top), with the absolute square of the gradient of the experimental data (bottom). The BZ and some symmetry points are also plotted.

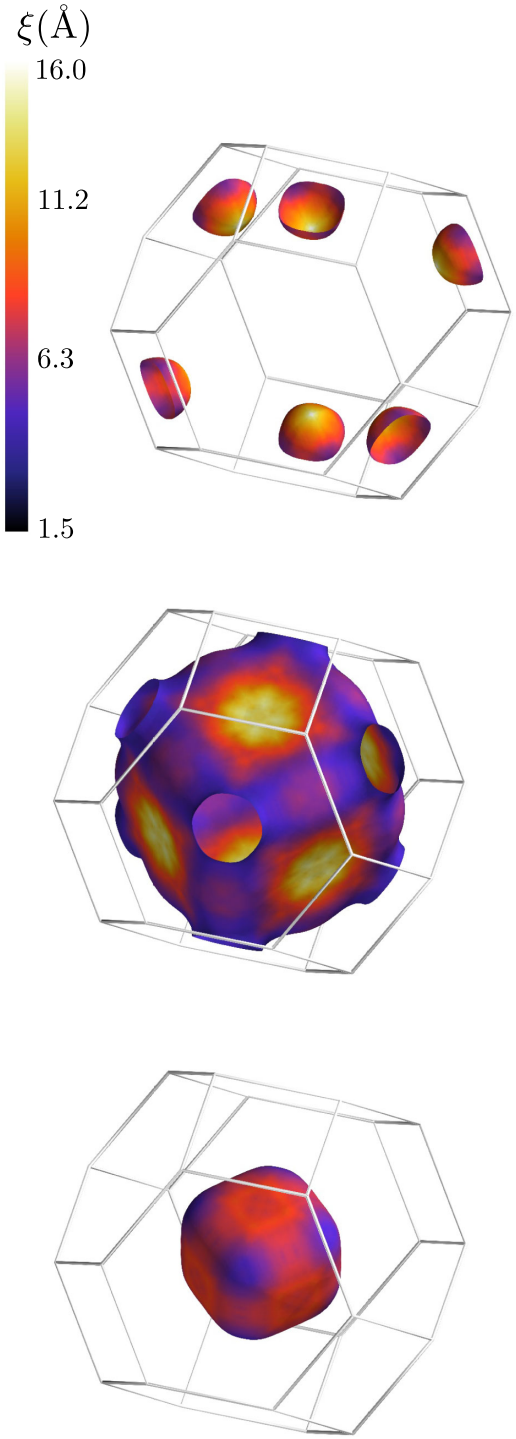

FIG. 4. The hole (top) and two electron (middle and bottom) FS sheets of NiFeCoCr obtained from the Compton experiment. These surfaces are the isodensities (0.5, 1.5, and 2.5) plotted from the reconstructed occupation number. The color shows the variation of the quasiparticle coherence length ξ (in Å) across the FS extracted from the smearing. The wireframe box is the first Brillouin zone.

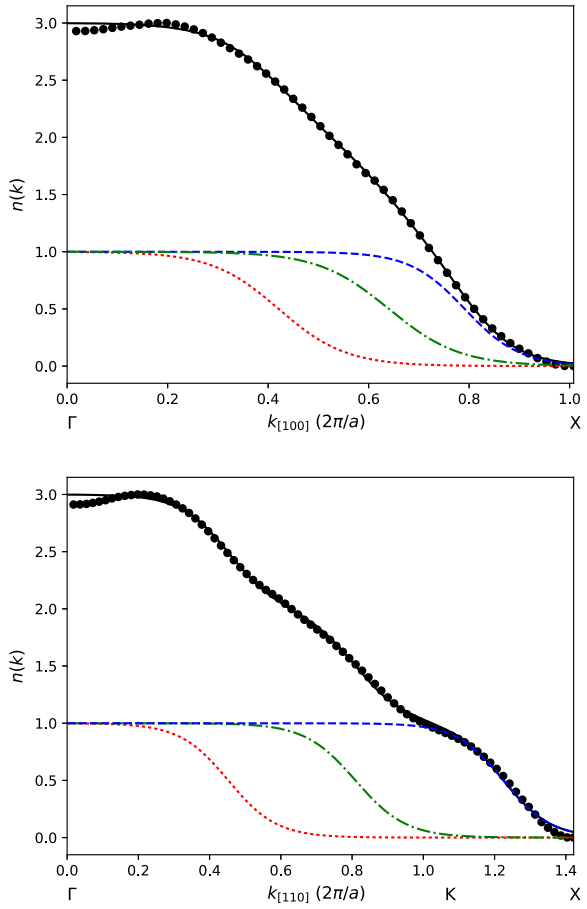

FIG. 5. Occupation $n(\mathbf{k})$ from the experiment (filled circles) along the [100] (top) and [110] (bottom) directions in the BZ (where k is in units of $2\pi/a$). $n(\mathbf{k})$ has been fitted with the sum (black line) of three tanh functions (red dotted line, green dashed-dotted line, and blue dashed line). The edge of the BZ is at 1.00 and 1.06 for the [100] and [110] directions, respectively, and symmetry points such as Γ, K, and X are shown.

the FS, it can be useful to look at a function related to the gradient of $n(\mathbf{k})$ [53]. This is applied to the experimental data and displayed in the bottom half of Fig. 3 where it can be seen that the least smeared regions (largest derivative) in the experimental data closely match the sharper BSF peaks in the KKR-CPA-DLM calculation shown in the top half of Fig. 3. The hole pockets at the X points are also revealed in the experimental data, the locus of the maximum of the gradient function showing that the sizes of the hole pockets are comparable with that predicted by the KKR-CPA-DLM theory, but even more smeared.

The isodensities can be used to visualize the full 3D FS topology from the Compton scattering experiment, as shown in Fig. 4. The larger Γ-centered electron sheet with necks along the $\langle 111 \rangle$ directions is reminiscent of the well-known FS of Cu [54] which originates from a free-electron-like band that emerges from the top of the d bands and intersects with the BZ boundary. The color of the iso-surfaces corresponds to the coherence length of the quasiparticles which has been evaluated through the method described below.

TABLE I. The surface area, mean free path (inferred from the smearing [26]), and resistivity ($12\pi^3\hbar/e^2\lambda\mathcal{A}$, see Ref. [26]) of each FS sheet.

FS sheet	Mean free path $\langle\lambda\rangle$ (nm)	FS area $\mathcal{A}$ ($\times 10^{17}$ cm^{-2})	Resistivity ρ ($\mu\Omega$cm)
1	0.91	0.75	225
2	0.73	2.16	97
3	0.70	0.39	565

By fitting a series of smeared unit step functions to $n(\mathbf{k})$ along a set of special directions [55], it is possible to extract the degree to which each sheet of FS is smeared along each direction. Such fits are not expected to capture all the details (e.g., the dip close to the Γ point [26]), but are useful for quantifying the smearing (used to estimate the quasiparticle coherence length [26]). When visualizing the individual FS sheets, the isodensities extracted from the step function fits (0.45, 1.48, and 2.47) are very close to the canonical values used above. Corrections were made to the coherence lengths extracted from the fits by simulating the impact of finite experimental resolution on different degrees of smearing. The FS-averaged mean free paths were calculated from a set of special directions using the approach detailed by Kontrym-Sznajd and Dugdale [55]. Examples of fits to the [100] and [110] directions (high symmetry directions that are not part of the set of special directions) are shown in Fig. 5, where the experimental $n(\mathbf{k})$ has been fitted with three smeared unit step functions (represented by tanh functions) with the position and width of each being free parameters [26]. The smeared steps in Fig. 5 span up to 40% of $2\pi/a$.

A summary of the FS-averaged mean free paths, FS areas, and resistivities can be found in Table I. The conductivity is dominated by the second (Cu-like) FS sheet, and the variation of the quasiparticle coherence length across this FS sheet strongly resembles the variation of the Fermi velocity across the FS of Cu [56]. The resistivity scales inversely with the area of the FS and thus the differences between the sheets is dominated by the differences in their surface areas. Combining the contribution from all three sheets in parallel gives a resistivity of 61 $\mu\Omega$ cm. As a crosscheck, this value compares favorably with the residual resistivity of 77 $\mu\Omega$ cm measured by Jin *et al.* [57]. The residual resistivity predicted directly by the KKR-CPA calculations using the Kubo-Greenwood formalism [26] is 51 $\mu\Omega$ cm, increasing to 67 $\mu\Omega$ cm for the DLM state.

In conclusion, we have measured the FS of the equiatomic disordered alloy NiFeCoCr which exhibits significant smearing of up to ~40% of $2\pi/a$. Across some regions of the FS the quasiparticle coherence length is very close to

the nearest-neighbor distance, implying close proximity to the MIR limit where the usual picture of ballistically propagating quasiparticles is invalid [4]. Both strong electron-electron scattering (due to strong electron correlations) and strong electron scattering due to atomic disorder can push a material towards the MIR limit. Treating the former is challenging for theory, but the latter can be incorporated within the CPA [58]. High-entropy alloys might thus provide an environment in which some important aspects of transport physics, normally associated strongly correlated electrons, could be simulated by disorder physics. NiFeCoCr appears close to a regime where the conventional picture of a quasiparticle with a well-defined momentum being subjected to occasional scattering events breaks down, signalling the demise of the Fermi liquid. It is interesting to note that NiCoCr, NiFeCoCrMn, and NiFeCoCrPd all have residual resistivities which are higher than NiFeCoCr and all exhibit similar non-Fermi-liquid behavior [57]. An electron mean free path, obtained by averaging the coherence length of the quasiparticles over each FS sheet as inferred from the FS smearing, gives an estimated residual resistivity of $\sim 61\ \mu\Omega\,\mathrm{cm}$. We have confirmed the presence of significant FS smearing which has been predicted for some Cantor-Wu alloys [14]. We have shown that the FS in a metal whose properties are dominated by disorder can be accurately described by state-of-the-art theoretical approaches (density functional theory combined with the coherent potential approximation) which generalize the concept of a metallic FS to such materials. Finally, magnetic Compton scattering [59] could be a useful probe of the nature of magnetic order in these and other alloys (for example, probing ferrimagnetism [60] in hcp NiFeCoCrW [61]).

The original research data are available by following the link provided in Ref. [62].

The Compton scattering experiment was performed with the approval of the Japan Synchrotron Radiation Research Institute (JASRI, Proposal No. 2016A1323). H. A. R. and D. A. L. gratefully acknowledge the financial support of the UK EPSRC (EP/L015544/1), and the National Secretariat of Higher Education, Science, Technology and Innovation of Ecuador (SENESCYT), respectively. S. M., G. D. S., and G. M. S. acknowledge funding support by the Energy Dissipation and Defect Evolution (EDDE), an Energy Frontier Research Center funded by the U.S. Department of Energy (DOE), Office of Science, Basic Energy Sciences under Contract No. DE-AC05-00OR22725. S. B. D. would like to thank Dr Christopher Bell (Bristol) for valuable discussions.

*s.b.dugdale@bristol.ac.uk

[1] P. Hoch, Contemp. Phys. **24**, 3 (1983).
[2] J. M. Luttinger, Phys. Rev. **119**, 1153 (1960).
[3] S. Huotari, J. A. Soininen, T. Pylkkänen, K. Hämäläinen, A. Issolah, A. Titov, J. McMinis, J. Kim, K. Esler, D. M. Ceperley, M. Holzmann, and V. Olevano, Phys. Rev. Lett. **105**, 086403 (2010).
[4] N. E. Hussey, K. Takenaka, and H. Takagi, Philos. Mag. **84**, 2847 (2004).
[5] B. L. Gyorffy and G. M. Stocks, Phys. Rev. Lett. **50**, 374 (1983).
[6] I. Wilkinson, R. J. Hughes, Z. Major, S. B. Dugdale, M. A. Alam, E. Bruno, B. Ginatempo, and E. S. Giuliano, Phys. Rev. Lett. **87**, 216401 (2001).
[7] M. Yaqub and J. F. Cochran, Phys. Rev. **137**, A1182 (1965).
[8] D. Gall, J. Appl. Phys. **119**, 085101 (2016).
[9] D. Miracle and O. Senkov, Acta Mater. **122**, 448 (2017).
[10] B. Cantor, I. Chang, P. Knight, and A. Vincent, Mater. Sci. Eng. A **375–377**, 213 (2004).
[11] Z. Wu, H. Bei, F. Otto, G. Pharr, and E. George, Intermetallics **46**, 131 (2014).
[12] H. Song, F. Tian, Q.-M. Hu, L. Vitos, Y. Wang, J. Shen, and N. Chen, Phys. Rev. Mater. **1**, 023404 (2017).
[13] G. D. Samolyuk, S. Mu, A. F. May, B. C. Sales, S. Wimmer, S. Mankovsky, H. Ebert, and G. M. Stocks, Phys. Rev. B **98**, 165141 (2018).
[14] S. Mu, G. D. Samolyuk, S. Wimmer, M. C. Troparevsky, S. N. Khan, S. Mankovsky, H. Ebert, and G. M. Stocks, npj Comput. Mater. **5**, 1 (2019).
[15] F. Körmann, Y. Ikeda, B. Grabowski, and M. H. F. Sluiter, npj Comput. Mater. **3**, 36 (2017).
[16] P. Koželj, S. Vrtnik, A. Jelen, S. Jazbec, Z. Jagličić, S. Maiti, M. Feuerbacher, W. Steurer, and J. Dolinšek, Phys. Rev. Lett. **113**, 107001 (2014).
[17] S. B. Dugdale, Low Temp. Phys. **40**, 328 (2014).
[18] B. L. Gyorffy, A. J. Pindor, J. Staunton, G. M. Stocks, and H. Winter, J. Phys. F **15**, 1337 (1985).
[19] J. Staunton, B. L. Gyorffy, A. J. Pindor, G. M. Stocks, and H. Winter, J. Phys. F **15**, 1387 (1985).
[20] H. Ebert, The Munich SPR-KKR Package, Version 7, http://olymp.cup.uni-muenchen.de/ak/ebert/SPRKKR (2017).
[21] J. S. Faulkner and G. M. Stocks, Phys. Rev. B **21**, 3222 (1980).
[22] W. R. Fehlner and S. H. Vosko, Can. J. Phys. **54**, 2159 (1976).
[23] N. Hiraoka, M. Itou, T. Ohata, M. Mizumaki, Y. Sakurai, and N. Sakai, J. Synchrotron Radiat. **8**, 26 (2001).
[24] G. Kontrym-Sznajd and M. Samsel-Czekała, Appl. Phys. A **70**, 89 (2000).
[25] D. G. Lock, V. H. C. Crisp, and R. N. West, J. Phys. F **3**, 561 (1973).
[26] See Supplemental Material at http://link.aps.org/supplemental/10.1103/PhysRevLett.124.046402 for more details, which includes Refs. [27–52].
[27] H. Bei and E. George, Acta Mater. **53**, 69 (2005).
[28] P. M. Platzman and N. Tzoar, Phys. Rev. **139**, A410 (1965).
[29] P. Eisenberger and P. M. Platzman, Phys. Rev. A **2**, 415 (1970).
[30] E. Zukowski, in *X-ray Compton Scattering*, edited by M. J. Cooper, P. E. Mijnarends, N. Shiotani, N. Sakai, and A. Bansil (Oxford University Press, Oxford, 2004).
[31] N. Sakai, J. Phys. Soc. Jpn. **56**, 2477 (1987).

[32] F. Biggs, L. Mendelsohn, and J. Mann, At. Data Nucl. Data Tables **16**, 201 (1975).
[33] J. Korringa, Physica **13**, 392 (1947).
[34] W. Kohn and N. Rostoker, Phys. Rev. **94**, 1111 (1954).
[35] P. Soven, Phys. Rev. **156**, 809 (1967).
[36] B. L. Gyorffy, Phys. Rev. B **5**, 2382 (1972).
[37] A. Zunger, S.-H. Wei, L. G. Ferreira, and J. E. Bernard, Phys. Rev. Lett. **65**, 353 (1990).
[38] S.-H. Wei, L. G. Ferreira, J. E. Bernard, and A. Zunger, Phys. Rev. B **42**, 9622 (1990).
[39] A. van de Walle, CALPHAD: Comput. Coupling Phase Diagrams Thermochem. **33**, 266 (2009).
[40] A. van de Walle, M. D. Asta, and G. Ceder, CALPHAD: Comput. Coupling Phase Diagrams Thermochem. **26**, 539 (2002).
[41] A. van de Walle, P. Tiwary, M. M. de Jong, D. L. Olmsted, M. D. Asta, A. Dick, D. Shin, Y. Wang, L.-Q. Chen, and Z.-K. Liu, CALPHAD: Comput. Coupling Phase Diagrams Thermochem. **42**, 13 (2013).
[42] J. K. Dewhurst, S. Sharma, L. Nordstöm, F. Cricchio, F. Bultmark, and E. K. U. Gross, The ELK FP-LAPW code, Version 2.3.22, http://elk.sourceforge.net (2013).
[43] D. Ernsting, D. Billington, T. D. Haynes, T. E. Millichamp, J. W. Taylor, J. A. Duffy, S. R. Giblin, J. K. Dewhurst, and S. B. Dugdale, J. Phys. Condens. Matter **26**, 495501 (2014).
[44] J. P. Perdew and Y. Wang, Phys. Rev. B **45**, 13244 (1992).
[45] S. H. Vosko, L. Wilk, and M. Nusair, Can. J. Phys. **58**, 1200 (1980).
[46] G. Kontrym-Sznajd and M. Samsel-Czekała, J. Appl. Crystallogr. **44**, 1246 (2011).
[47] P. R. Tulip, J. B. Staunton, S. Lowitzer, D. Ködderitzsch, and H. Ebert, Phys. Rev. B **77**, 165116 (2008).
[48] R. Kubo, J. Phys. Soc. Jpn. **12**, 570 (1957).
[49] D. A. Greenwood, Proc. Phys. Soc. **71**, 585 (1958).
[50] Z. Szotek, B. L. Gyorffy, G. M. Stocks, and W. M. Temmerman, J. Phys. F **14**, 2571 (1984).
[51] Y.-F. Kao, S.-K. Chen, T.-J. Chen, P.-C. Chu, J.-W. Yeh, and S.-J. Lin, J. Alloys Compd. **509**, 1607 (2011).
[52] K. Jin, S. Mu, K. An, W. Porter, G. Samolyuk, G. Stocks, and H. Bei, Mater. Des. **117**, 185 (2017).
[53] J. A. Weber, D. Benea, W. H. Appelt, H. Ceeh, W. Kreuzpaintner, M. Leitner, D. Vollhardt, C. Hugenschmidt, and L. Chioncel, Phys. Rev. B **95**, 075119 (2017).
[54] A. B. Pippard, Phil. Trans. R. Soc. A **250**, 325 (1957).
[55] G. Kontrym-Sznajd and S. B. Dugdale, J. Phys. Condens. Matter **27**, 435501 (2015).
[56] M. Gradhand, D. V. Fedorov, F. Pientka, P. Zahn, I. Mertig, and B. L. Györffy, Phys. Rev. B **84**, 075113 (2011).
[57] K. Jin, B. C. Sales, G. M. Stocks, G. D. Samolyuk, M. Daene, W. J. Weber, Y. Zhang, and H. Bei, Sci. Rep. **6**, 20159 (2016).
[58] G. D. Samolyuk, C. C. Homes, A. F. May, S. Mu, K. Jin, H. Bei, G. M. Stocks, and B. C. Sales, Phys. Rev. B **100**, 075128 (2019).
[59] J. A. Duffy, J. Phys. Conf. Ser. **443**, 012011 (2013).
[60] T. D. Haynes, I. Maskery, M. W. Butchers, J. A. Duffy, J. W. Taylor, S. R. Giblin, C. Utfeld, J. Laverock, S. B. Dugdale, Y. Sakurai, M. Itou, C. Pfleiderer, M. Hirschberger, A. Neubauer, W. Duncan, and F. M. Grosche, Phys. Rev. B **85**, 115137 (2012).
[61] R. Lizárraga, E. Holmström, and L. Vitos, Phys. Rev. Mater. **2**, 094407 (2018).
[62] S. B. Dugdale, University of Bristol Research Data Repository, https://doi.org/10.5523/bris.1a9u533pcxzk23lbwu1p56ica (2019).